26th EPS Conf. on Contr. Fusion and Plasma Physics, Maastricht, 14 - 18 June 1999 ECA Vol.23J (1999) 785 - 788

Non-linear magnetic reconnection due to external forcing.

G. Valori, H.J. de Blank, J. Rem, and T.J. Schep.

FOM-Instituut voor Plasmafysica, Association Euratom-FOM,
Trilateral Euregio Cluster, P.O. Box 1207, 3430 BE Nieuwegein, The Netherlands

Introduction. Hamiltonian reconnection is nowadays believed to provide a plausible explanation for fast magnetic topology changes in hot plasmas, where the time scale of the magnetic activity is found to be smaller than the resistive reconnection time scale. The numerical work presented here is focused on the general case of a forced system. The reconnection process driven by a displacement of the walls embedding a plasma slab is numerically investigated in the resistive case and in the Hamiltonian case. In the latter case, the magnetic field topology is changed due to electron inertia. The adopted model [1] includes the Hall term in the generalized Ohm law, a term which arises due to the coupling between the electron parallel compressibility and the ion motion. Finite ion gyro-radius and asymmetric forcing effects are also discussed.

The model. The model of Ref. [1] is adopted, where the reduced magneto-hydrodynamic (RMHD) model of a plasma slab considered in Refs. [2], [3] is extended by including electron inertia and finite pressure effect in Ohm's law. Electron inertia, instead of resistivity, is then responsible for magnetic field topology changes. The model is valid when the scale lengths of both the equilibrium and the perturbations are much smaller than the radius of curvature and the equilibrium density scale length. In this limit, excluding the compressional Alfvén waves, a simple representation of the magnetic field can be adopted. Introducing the magnetic flux ψ and electric potential ϕ, the electro-magnetic fields can be described by $\boldsymbol{B} = B_0(\boldsymbol{e}_z + \boldsymbol{e}_z \times \nabla\psi)$, and $\boldsymbol{E} = (B_0/c)(-\nabla\phi + \boldsymbol{e}_z\partial_t\psi)$, where $\boldsymbol{e}_z$ is the unit vector in the z direction. Assuming z, the toroidal coordinate, to be ignorable, the model describes a reduced, 2D, configuration. We consider a strongly magnetized, low-β plasma, where the perturbation scale-length in the directions perpendicular to $\boldsymbol{B}$ are much smaller than the perturbation scale-length in the direction parallel to $\boldsymbol{B}$. The ion dynamics is described in a small-ρ_i expansion of the ion model in Ref. [1], namely $\omega = \nabla_\perp^2(\phi + \rho_i^2\omega)$, where ω is the ion vorticity and ρ_i the ion gyro-radius. The quasi-neutrality condition couples the ion density perturbations with the electron compressibility in the parallel motion, leading to the reduced system of equations

$$\begin{aligned} \partial_t\omega + [\phi,\omega] - v_A^2\,[\psi, J] &= \nu_i\nabla_\perp^2\omega, \\ \partial_t\psi + \left[\phi - \rho_s^2\omega, \psi\right] &= d_e^2\,(\partial_t J + [\phi, J]) + \eta J, \\ \omega = \nabla_\perp^2(\phi + \rho_i^2\omega), \qquad J &= \nabla_\perp^2\psi, \end{aligned} \tag{1}$$

where $v_A \equiv B_0(4\pi n m_i)^{-1/2}$ is the Alfvén velocity, $\rho_s = \rho_i\sqrt{T/T_i}$ the ion sound gyro-radius, $d_e = c/\omega_e$ the electron inertia skin depth, ω_e the electron plasma frequency, ν_i the ion viscosity, η the resistivity, and $[\ ,\ ]$ the perpendicular Jacobian. The current density J and the magnetic flux ψ are related by Ampère's law.
Neglecting the collisional terms, in the cold ion limit ($\rho_i \to 0$) the Hamiltonian structure

of Eqs.(1) can be revealed by defining two fluxes $G_\pm \equiv \psi - d_e^2 J \pm \rho_s d_e \omega$. They are passively advected by the flow fields of the stream functions $\Phi_\pm \equiv \phi - \rho_s^2 \omega \pm \rho_s d_e J$,

$$\partial_t G_\pm + [\Phi_\pm, G_\pm] = 0. \tag{2}$$

Equations (2) and their conservation properties are extensively analyzed elsewhere [1, 4, 5].

Numerical results. All numerical results presented here are obtained with the vectorized code *Vlugr2* [6] which employs a 2^{nd} order implicit finite-difference method and uses adaptive, local uniform grid refinement. The high resolution provided by the adaptive grid refinement technique is needed in order to resolve small scale structures that appear in the late non-linear stage of the reconnection process.
The magnetic configuration is a plasma slab ($-L_x \leq x \leq L_x, -L_y \leq y \leq L_y$) in static equilibrium with a neutral line in $x = 0$ ($\psi = \frac{1}{2}x^2$, $\phi = 0$ as initial conditions), confined in the x direction by two flux conserving walls and periodic in the y direction. The system is excited by a displacement of the walls at $x = \pm L_x$, given by $x = \pm L_x \mp \delta_{wall} \cos(my) \tanh(t/\tau_{wall})$, where $m = \pi/L_y$, $\delta_{wall} = 0.04$, $\tau_{wall} = 10$, $L_x = 1$, and $L_y = 10$ are the used parameters. Time is normalized to the Alfvén time. The walls moves for a finite interval of time and excite Alfvén waves inside the system. The question of the dynamical evolution of the system is known in literature as Taylor's problem [2]. Sections $I - IV$ refer to numerical results obtained for different values of the parameters appearing in Eqs. (1).
Resistive reconnection ($d_e = \rho_s = \rho_i = \nu_i = 0$). In the RMHD limit resistivity is responsible for magnetic field line reconnection. The linear reconnection regime in the RMHD limit has been studied in [2]. The non-linear regime was investigated numerically in [3], from which the following observations are taken. In the X point $\partial_t \psi = \eta J$. Hence, relatively small variations of the island width correspond to rather big increments of the current maximum. The reconnection process generates a current sheet along the neutral line, whose maximum grows exponentially in time. The width of the current channel is limited by diffusion, depending on the resistivity as $\eta^{1/2}$. The whole process can be recognized as Sweet-Parker reconnection [3].
I **Hamiltonian reconnection** (numerical results for $d_e = 0.18$, $\rho_s = \rho_i = 0$, $\nu_i = 10^{-4}$, $\eta = 0$). When the temperature is so high that resistivity is less effective, electron inertia is considered instead. Also in this case the current density forms a sheet along the neutral line (see Fig. 2(a)). Because in the X point $\partial_t(\psi - d_e^2 J) = 0$, the term $d_e^2 \partial_t J$ has to balance the time evolution of ψ, *i.e.* of the reconnected flux. So both ψ and J evolve as shown in Fig. 1(a). Note that the reconnection layer is of the order of d_e, and that the island can grow beyond this width, as shown in Fig. 1(d).
II **Ion sound gyro-radius effects** (numerical results for $d_e = \rho_s = 0.18$, $\rho_i = 0$, $\nu_i = 10^{-5}$, $\eta = 0$). In the limit of non-vanishing electron temperature the density perturbations are related to the electric potential via the ion sound gyro-radius ρ_s. This additional scale length can be viewed as modifying the advection of ψ in the momentum balance equation. This has three consequences. First, the current is now distributed in two layers intersecting each other at the X point, similar in shape, but not identical, to the separatrix (see Fig. 2(b)). In fact, this structure has been understood in [4] as being a result of the opposite advection of the generalized fluxes $G_\pm$ by the corresponding

generalized stream functions $\Phi_{\pm}$. Indeed, this can happen only for non-vanishing ρ_s. Second, the growth rate is increased. In Fig. 1(a) the behavior of the current maximum is shown; as in case I, the same behavior holds for the reconnected flux. The long time evolution of the island width in Fig. 1(c) shows that it reaches a maximum, after which an oscillatory regime is entered. Third, a dramatic scale collapse takes place in the current density, generating a current peak in the X point whose width shrinks below d_e and ρ_s by several orders of magnitude. The width of the current peak in the x direction is measured as $l_x = (J(t=0)/\partial_x^2 J(t))^{1/2}\big|_X$. Its temporal behavior is drawn in Fig. 1(b). If no dissipation is present, the collapse can span five orders of magnitude. The diffusive effect of ion viscosity stops the collapse but the formed sub-layer structures survive, as in Fig. 1(b). These results have also been analyzed in [7] and [8] for the forced system, and in [5] for the unstable one. A comparison between the two cases is discussed in [9].

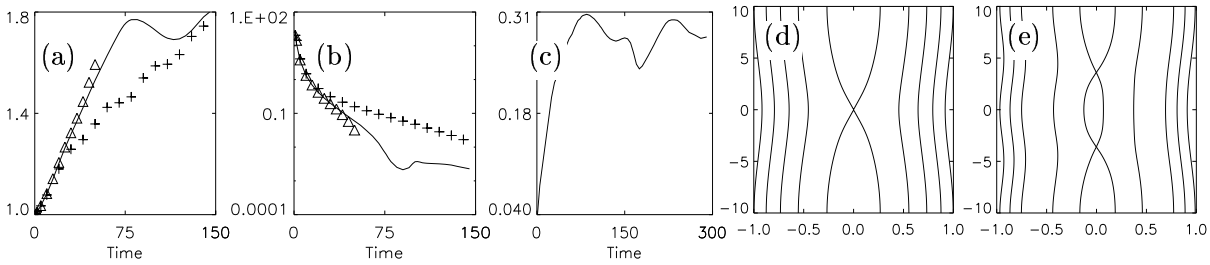

Figure 1: *Time evolution of (a) current density in the X point; (b) l_x on logarithmic scale; for case I (crosses), II (continuous line), and III (triangles); (c) half island width in II; (d) isolines of ψ at $t = 110$ in I; (e) isolines of ψ at $t = 110$ in IV.*

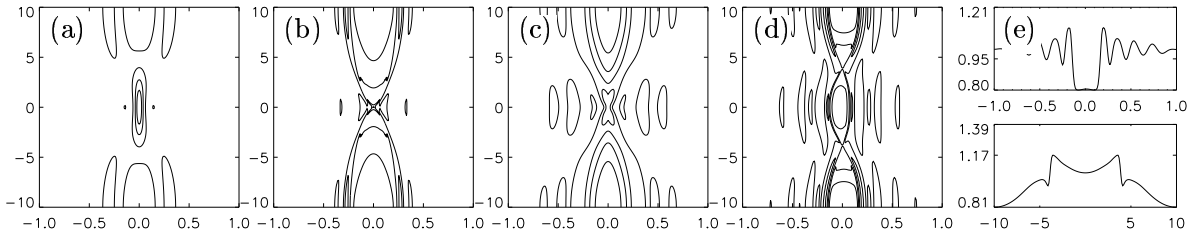

Figure 2: *Isolines of the current density for case I at $t = 110$ (a), II at $t = 110$ (b), III at $t = 55$ (c), and IV at $t = 110$ (d); (e) top and bottom: current density on sections along $x = 0$ and $y = 0$ in figure (d), respectively.*

III **Ion gyro-radius effects** (numerical results for $d_e = 0.18$, $\rho_s^2 = \frac{2}{3}d_e^2$, $\rho_i^2 = \frac{1}{3}d_e^2$, $\nu_i = 10^{-5}$, $\eta = 0$). When also finite ion temperature is considered, the vorticity equation is modified. In the linearized equations, the ion gyro-radius enters only in combination with ρ_s as $(\rho_s^2 + \rho_i^2)^{1/2}$. In Figs. 1(a,b) the time evolution of the current maximum and l_x is shown for values of d_e and $(\rho_s^2 + \rho_i^2)^{1/2}$ that are the same as d_e and ρ_s in case II. The current distribution, Fig. 2(c), is the same as in case II. In the time interval in Fig. 1(a) the evolution of the current maximum in cases II and III cannot be distinguished. The same holds for l_x: the scale collapse is not affected by ion temperature. Ion gyro-radius effects for an unstable configuration are presented in [10].

IV **Asymmetric forcing** (parameters as case II). Cases $I - III$ are perfectly symmetric. In order to see if the scale collapse takes place under more generic conditions, we have considered an asymmetric configuration. On the boundary at $x = L_x$ the same

forcing is applied as before, while at $x = -L_x$ an $m = 2$ mode (with the same temporal dependence and amplitude) is now used. This wall modulation is evident in the isolines of ψ shown in Fig. 1(e). As a consequence of the $m = 2$ modulation, two X points are formed. Figure 2(d) is a contour plot of the current density at $t = 110$. No current peaks with widths much smaller than d_e and ρ_s are formed. The current density profiles between the X points shown by the sections of J along $x = 0, y = 0$ in Fig. 2(e) present rather steep gradients, but no scale collapse is taking place there.

Conclusions. Numerical simulations of resistive as well as of Hamiltonian forced reconnection in two fluid models have been presented. In the collisionless case, effects of electron inertia, electron and ion temperature have been discussed. Numerical results show the formation of magnetic islands whose widths are comparable or bigger than the intrinsic plasma scale-lengths, namely the electron inertia skin depth and the ion sound gyro-radius. When the island growth comes to an end an oscillatory regime is entered. Simulations show that, in the time interval considered here, no significative effect arises from the inclusion of the ion temperature $T_i = \frac{1}{2}T_e$ in the model. In all cases of symmetric forcing, rapidly narrowing micro-scale structures are observed in the current density near the X point. The question arises whether this scale collapse gives rise to a finite-time singularity. It turns out that finite time collapses are not present in the cases we reported [11]. A main result of this work is that the small scale structures generated close to the X point in the current density by the reconnection process survive indefinitely, even when ion viscosity is included in the model. Asymmetric forcing has also been studied. In this case, no scale collapse takes place.

Acknowledgments. The authors are pleased to thank F. Califano, D. Grasso, M. Ottaviani, F. Pegoraro and F. Porcelli for fruitful discussions. This work was performed under the Euratom-FOM Association agreement with financial support from NWO and Euratom.

References

[1] T.J. Schep, F. Pegoraro, B.N. Kuvshinov, Phys. Plasmas **1** 2843 (1994).

[2] T.S. Hahm, R.M. Kulsrud, Phys. Fluids **28** 2412 (1985).

[3] J. Rem, T.J. Schep, Plasma Phys. and Control. Fusion **40** 139 (1998).

[4] E. Cafaro, D. Grasso, F. Pegoraro, F. Porcelli, A. Saluzzi, Phys. Rev. Lett. **80** 4430 (1998).

[5] D. Grasso, F. Pegoraro, F. Porcelli, F. Califano, submitted to Phys. Rev. E

[6] J.G. Blom, R.A. Trompert, J.G. Verwer, ACM Trans. Math. Soc. **22** 302 (1996).

[7] G. Valori, H.J. de Blank, J. Rem, T.J. Schep, *Proceedings of the Joint Varenna – Lausanne international workshop on "Theory of Fusion Plasmas"*, Varenna, 1998, (Editrice Compositori, Bologna, 1999), p. 555 .

[8] H.J. de Blank, J. Rem, G. Valori, in *Proceedings of the 25th European Conference on Controlled Fusion and Plasma Physic*, Praha (1998), Europ. Conf. Abs. Vol. 22C, p. 2188

[9] G. Valori, D. Grasso, H.J. de Blank, submitted to Phys. Plasmas.

[10] D. Grasso, F. Califano, F. Pegoraro, F. Porcelli, "Collisonless magnetic reconnection.", these Proceedings.

[11] H.J. de Blank, J. Rem, G. Valori "Finite time singularities and regular motion in magnetic reconnection", these Proceedings.